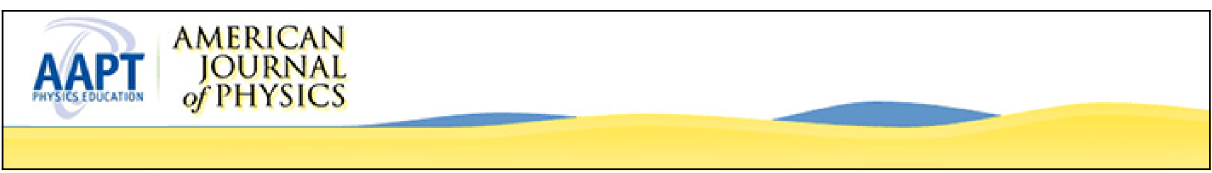

Scanning capacitance microscopy using a relaxation oscillator

M. Pahlmeyer, A. Hankins, S. Tuppan, and W. J. Kim

Citation: American Journal of Physics **83**, 104 (2015); doi: 10.1119/1.4899045
View online: http://dx.doi.org/10.1119/1.4899045
View Table of Contents: http://scitation.aip.org/content/aapt/journal/ajp/83/2?ver=pdfcov
Published by the American Association of Physics Teachers

Articles you may be interested in
Intermittent contact scanning nonlinear dielectric microscopy
Rev. Sci. Instrum. **81**, 023705 (2010); 10.1063/1.3274138

Fiber laser relaxation oscillation noise suppression through the use of self-biased intracavity loss modulator
J. Appl. Phys. **96**, 1790 (2004); 10.1063/1.1773919

Observation of subsurface monolayer thickness fluctuations in InGaN/GaN quantum wells by scanning capacitance microscopy and spectroscopy
Appl. Phys. Lett. **85**, 407 (2004); 10.1063/1.1773358

Microwave-mixing scanning capacitance microscopy of pn junctions
J. Appl. Phys. **86**, 7094 (1999); 10.1063/1.371797

Scanning Joule expansion microscopy at nanometer scales
Appl. Phys. Lett. **72**, 37 (1998); 10.1063/1.120638

This article is copyrighted as indicated in the article. Reuse of AAPT content is subject to the terms at: http://scitation.aip.org/termsconditions. Downloaded to IP: 66.194.72.20 On: Thu, 22 Jan 2015 23:42:23

Scanning capacitance microscopy using a relaxation oscillator

M. Pahlmeyer, A. Hankins, S. Tuppan, and W. J. Kim[a)]
901 12th Avenue, Department of Physics, Seattle University, Seattle, Washington 98122

(Received 10 January 2014; accepted 10 October 2014)

We have performed scanning capacitance microscopy using a relaxation oscillator. Precision calibrations indicate a sensitivity on the order of 0.05 pF. Surface topography of metallic structures, such as machined grooves and coins, can be readily obtained either in the constant-height (non-contact) or tapping (contact) mode. Spatial resolution of less than 50 μm has been achieved. Our simple, low-cost system can be a valuable platform in the undergraduate laboratory, providing students with experience in microscopic imaging techniques. © *2015 American Association of Physics Teachers.*
[http://dx.doi.org/10.1119/1.4899045]

I. INTRODUCTION

Scanning capacitance microscopy (SCM) is a useful imaging technique that enables one to acquire topographical features of micro- and nano-sized samples. One of the early SCM instruments, based upon a commercial product (the RCA CED video disc),[1] is made of a capacitive sensor driven by an ultra-high-frequency oscillator (500 MHz or higher), a sharp tip, and a sample to be imaged, all of which are in a feedback loop to maintain a maximum resonant output. Primary applications include surface characterizations of nano structures[2,3] and the profiling of both conductors and insulators, particularly to acquire semiconductor (*p*- and *n*-type) dopant density profiles,[4,5] with sub-100-nm resolution. More recently, researchers have developed an integrated capacitance bridge for enabling quantum capacitance measurements at room temperature.[6]

SCM uses what is essentially a near-field capacitive sensor providing either the direct tip-sample capacitance (C), or its gradient with respect to the tip-sample separation (dC/dx), the latter being a more common choice for imaging due to its high sensitivity achieved by a lock-in technique. Therefore, it is easy to recognize SCM as a variant of atomic force microscopy (AFM), since the tip-sample electric *capacitance* is directly related to the tip-sample electric *force*, which is proportional to the gradient of the capacitance itself. For this reason, SCM is frequently employed as another operating mode of atomic force microscopes, providing a direct measure of classical electrostatics between a tip and the surface of a sample.

Previously, we have reported the usefulness of a relaxation oscillator for measuring the capacitance between two metal plates in an attempt to characterize the absolute separation between them.[7,8] Here, we extend our capacitance measurements to a topological mapping of the surface of a sample in both contact and non-contact modes. Our simple, low-cost SCM provides a valuable experimental platform in the undergraduate laboratory where students gain critical exposure to basic elements of scanning probe microscopy (SPM) techniques. We present precision calibrations of the relaxation oscillator, and successful two-dimensional surface scans of machined grooves and American coins.

II. RELAXATION OSCILLATOR

The relaxation oscillator, shown in the top of Fig. 1, consists of a comparator, an external capacitance to be measured, and three resistors. In our previous application,[7] there was an internal capacitor $C_{\rm int} = 47$ pF connected to $C_{\rm ext}$ in parallel; however, in the present oscillator, only the capacitance of an external source—plus possible parasitic

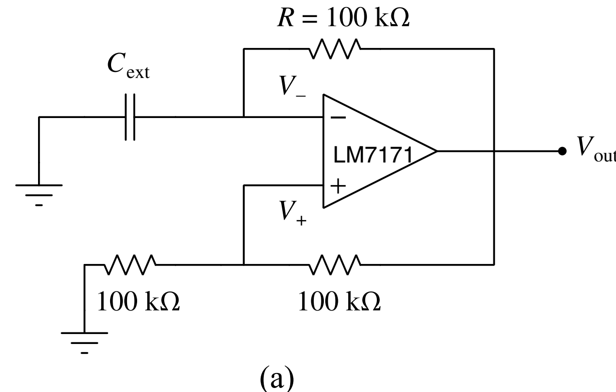

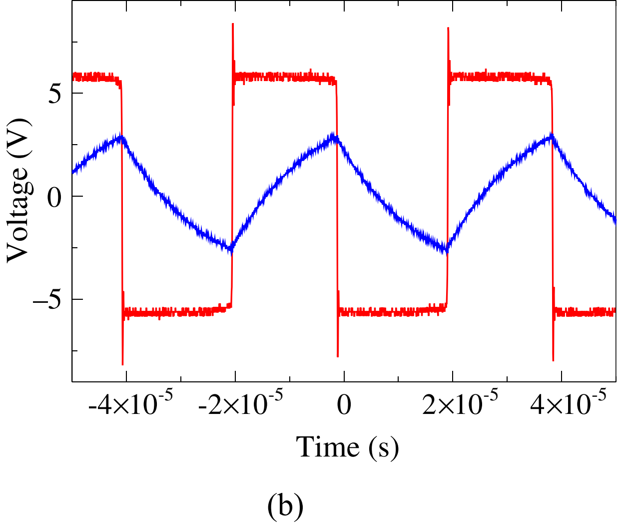

Fig. 1. Circuit diagram of a relaxation oscillator (top) and a plot of the oscillator and capacitor outputs, $V_{\rm out}$ (square wave) and V_- (RC charging-discharging cycle), respectively, captured by an oscilloscope (bottom). The total capacitance can be expressed as $C = C_{\rm ext} + C_{\rm para}$, where $C_{\rm para}$ represents possible parasitic capacitance present in the external wiring. Together with the 100 kΩ resistor, the RC charging-discharging cycle is established. When $V_{\rm out}$ is set to positive ($+V_0$), $C_{\rm ext}$ is charged to a set voltage $V_0/2$, according to the 1:1 voltage divider. Once it exceeds the set voltage, $V_{\rm out}$ flips to negative ($-V_0$), and discharging follows, with V_- becoming more negative until $V_+ > V_-$; at this point $V_{\rm out}$ flips back to positive, thereby competing one full cycle.

This article is copyrighted as indicated in the article. Reuse of AAPT content is subject to the terms at: http://scitation.aip.org/termsconditions. Downloaded to IP: 66.194.72.20 On: Thu, 22 Jan 2015 23:42:23

capacitance—contributes to the characteristic oscillation period set by the RC constant, where R is the $100\,\mathrm{k}\Omega$ resistor above the negative input of the op-amp. The other two $100\,\mathrm{k}\Omega$ resistors, just below the positive input of the op-amp, act as a voltage divider, with V_+ being just half of the maximum output of the oscillator V_{out}. The total "capacitance" of the circuit, combining both C_{ext} and parasitic capacitance, repeats charging-discharging cycles at V_-, which result in square waves at the oscillator output, as shown in the bottom of Fig. 1.

To understand the circuit qualitatively, let us assume that V_{out} is initially held at a constant maximum voltage V_0. At this point, V_+ is exactly $1/2V_0$. The external capacitor then starts charging up and the voltage increases at V_-. Note that, as long as $V_- < V_+$, the output remains constant at V_0, and that the voltage across the capacitor keeps on increasing until $V_- > V_+$, at which point the oscillator output swings to $-V_0$. Once the oscillator output flips, the capacitor starts discharging. As long as the output remains at $-V_0$, the capacitor continues to discharge until $V_+ > V_-$, at which point the cycle repeats itself.

Quantitatively, we can derive the relationship between the period of the oscillation and the RC time constant.[9] Applying Kirchhoff's rule and Ohm's law to the RC components of the op-amp, we have $V_{\mathrm{out}} = V_- + V_R$, where V_R is the voltage drop across the resistor. This leads to

$$V_{\mathrm{out}} - V_- = RC\frac{dV_-}{dt}, \tag{1}$$

where C is the total capacitance of the system and $R = 100\,\mathrm{k}\Omega$. The period T of the oscillation can be calculated by considering one half-period during which the capacitor output at V_- swings from $-1/2V_0$ to $+1/2V_0$. Solving Eq. (1) with initial conditions (i) $V_- = -V_0/2$, and (ii) $V_{\mathrm{out}} = V_0$ at $t = 0$, yields

$$V_- = V_0\left(1 - \frac{3}{2}e^{-t/RC}\right). \tag{2}$$

The time elapsed when V_- reaches $+1/2V_0$ is exactly a half-period ($t = T/2$), so the period of the oscillation is immediately obtained as

$$T = 2\ln(3)RC. \tag{3}$$

A few remarks are in order with regard to Eq. (3). First, the period of the relaxation oscillator is directly proportional to the capacitance being measured. To give a rough estimate, for $C = 10$ pF and $R = 100\,\mathrm{k}\Omega$, a typical period to be measured is on the order of $10\,\mu$s (see Sec. III). Second, Eq. (3) contains the dc offset (i.e., T_0 or baseline value of T) due to the parasitic capacitance. That is, $T = 2\ln(3)R(C_{\mathrm{ext}} + C_{\mathrm{para}})$, where the total capacitance is the sum of the variable external capacitance and the fixed parasitic capacitance originating from the circuit wiring and other contacts. Thus, by defining the offset value $T_0 \equiv 2\ln(3)RC_{\mathrm{para}}$, Eq. (3) can be re-expressed as

$$T = T_0 + 2\ln(3)RC_{\mathrm{ext}}. \tag{4}$$

To obtain rough estimates of resolution related to differential capacitance, we take the inverse of the derivative of Eq. (4) with respect to C_{ext}

$$\frac{\partial C_{\mathrm{ext}}}{\partial T} = \frac{1}{2\ln(3)R}, \tag{5}$$

which gives an expected calibration factor of $\alpha \approx 5$ pF/μs. For a 100 MHz (or 0.01 μs) counter, the lower bound of capacitance sensitivity is 0.01 pF, which is compatible to or even better than some commercially available RCL meters. In reality, the actual sensitivity is limited by drifts in measurements, such as those caused by temperature and acoustic vibrations, as noticed in our own measurements (see Sec. IV).

In selecting an op-amp, slew rate is an important consideration as the oscillator output rapidly swings between two extrema (e.g., positive to negative). We have chosen the LM7171 as a comparator due to its fast slew rate (4100 V/μs) and low-noise performance (14 nV/$\sqrt{\mathrm{Hz}}$). Our previous choice, the OP27, despite its lower noise performance (3 nV/$\sqrt{\mathrm{Hz}}$), has a slew rate of only about 3 V/μs, which overrides the lower bound of capacitance set by the counter. Other options, such as the AD790 and the AD8561, that are specifically designed to operate as comparators, provide ultra-fast rise and fall time on the order of nanoseconds. Another approach for building a relaxation oscillator has been proposed by Liu *et al.*[10] In their configuration, the oscillator operates on two op-amps, one as an integrator for active measurements of the RC constant and the other as a comparator to measure the charging-discharging cycle. While the two approaches are equally viable, we have chosen the single-comparator configuration because of its stable outputs and its simplicity.

III. EXPERIMENTAL SETUP AND CALIBRATIONS

To perform scanning capacitance microscopy, a stage is constructed with three mechanical actuators (two Z825BV and one Z812BV from Thorlabs), which move in the three Cartesian axes, as shown in Fig. 2. Each actuator has 50 nm resolution and travel ranges of 25 mm and 12 mm in lateral and vertical translations, respectively. It is important to ensure good insulation and rigid placement of various parts in the vicinity of tip and sample, because the relaxation oscillator is extremely delicate. For example, it can be disturbed by a tiny capacitance as a result of walking near the circuit. We have used a glass tube (Vitro tube) to secure the probe tip, and the various wires connecting to the relaxation

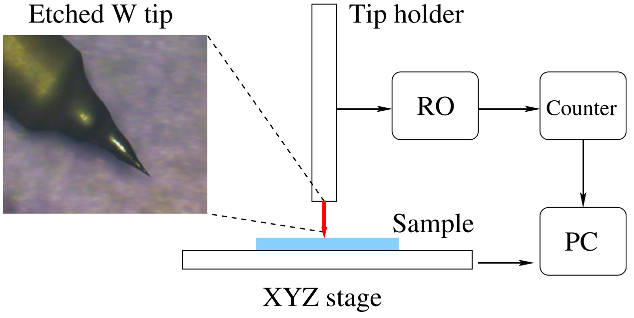

Fig. 2. Schematic of the experimental setup. The XYZ stage is controlled by the PC to move in relation to the probe tip, which is held at a fixed location in space. The sample and the probe tip form C_{ext} and consequently determine the period of the relaxation oscillator (RO). The period is measured by the counter (Keithley 2015 THD Multimeter) and collected by the PC via a MATLAB data acquisition program. The etched tungsten has a tip size on the order of 2 μm, which can be readily estimated from the initial diameter of the non-etched wire of 500 μm (see inset).

This article is copyrighted as indicated in the article. Reuse of AAPT content is subject to the terms at: http://scitation.aip.org/termsconditions. Downloaded to IP: 66.194.72.20 On: Thu, 22 Jan 2015 23:42:23

oscillator are kept as short as possible to further minimize interference.

The probe tip is electrochemically etched on a tungsten wire in 2 M sodium hydroxide inside a teflon cell.[12,13] A positive electrode (+2 V) is connected to the top of the tungsten wire with a negative electrode (ground) in the solution. The electrical energy coupled with the basic solution induces effective etching during which the wire surrounded by the meniscus is etched slower than the wire deeper in the solution. Because of this, the tungsten wire becomes thinner towards the tip. The process continues until the weight of the base of the wire exceeds the tensile strength of the etched portion of the wire. When the base falls off, it leaves a sharp needle-like tip, as shown in Fig. 2. Alternatively, a paperclip can be used as a probe tip by cutting the end diagonally, which also produces a relatively sharp tip point.

To calibrate the relaxation oscillator, we used a number of precision capacitors (Vishay Sprague 5% tolerance), across a range of capacitance values from 1 to 100 pF. This direct calibration, shown in the top of Fig. 3, gives $T_0 = (5.2 \pm 1.0)$ μs

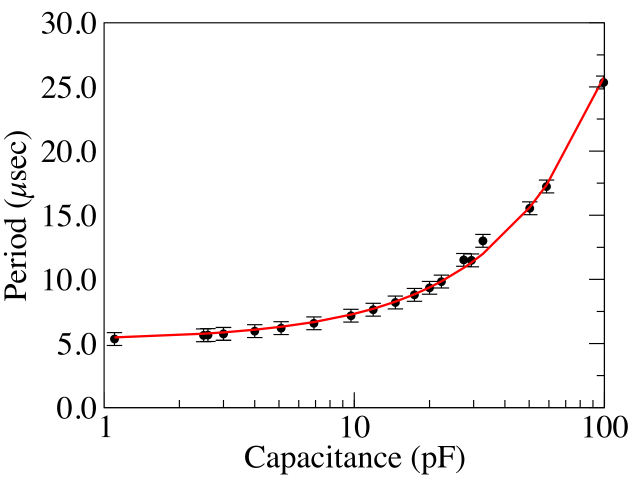

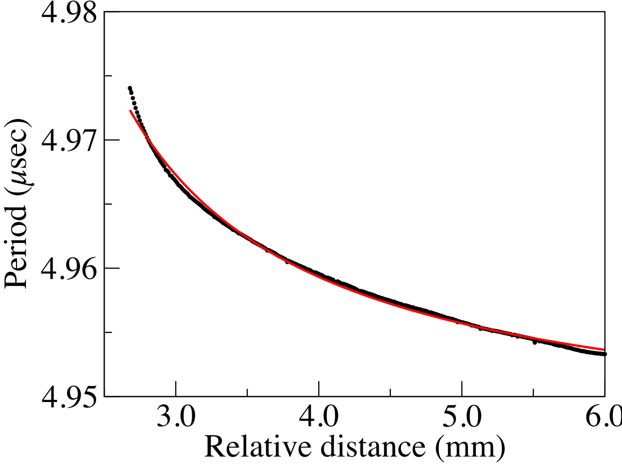

Fig. 3. Direct calibration using precision capacitors of known capacitance (top) and parallel-plate calibration by mapping the periods at different separation distances between the probe tip and the sample surface (bottom). By fitting the data from the direct calibration to a linear function (i.e., first-order polynomial), we obtain a period-to-capacitance calibration factor $\alpha = (4.87 \pm 0.75)$ pF/μs. The parallel-plate calibration is somewhat imprecise, because the tip-sample geometry is not precisely known *a priori*. The deviation from the $1/d$ fit (i.e., the solid red fitting curve falls short at short distances) is evident as the tip-probe separation is decreased.

and the calibration factor $\alpha = (4.87 \pm 0.75)$ pF/μs, consistent with the expected value calculated from Eq. (5). The calibration factor enables a conversion of period in seconds (s) to the actual unit of capacitance (F). From the standard deviation of the mean (SDOM) of $N = 50$ measurements, our oscillator reaches a resolution of 0.001 pF in about 3 s. We have also confirmed the capacitance of the precision capacitors using an RCL meter (Fluke PM6303A).

An alternative way to calibrate the relaxation oscillator is to employ a parallel-plate system in which capacitance is expected to obey $C_{ext} = \epsilon_0 A/d$ (with A being the effective area of the system) and then to fit the resulting data with a power-law form $T = T_0 + \beta/(d_r - d_0)^\gamma$, where T_0 is the offset period, d_0 is a point of contact, d_r is the relative distance recorded by the actuator steps, and $\gamma = 1$ (see Appendix B for details). The pre-factor, β, is directly related to physical parameters, such as ϵ_0 and A. The bottom of Fig. 3 is generated by first bringing the tip almost in contact with the sample, in this case to a distance of approximately 100 μm, and then stepping further away in increments of 1 μm until it reaches a maximum distance determined by the range of the linear actuator. The graph, though strongly displaying the $1/d$ relationship at larger distances (i.e., away from the other plate), suffers a severe deviation from the expected power law at short distances, possibly due to deviation from parallelism (i.e., $\gamma \neq 1$). For this reason, the $1/d$ calibration is not as reliable as the direct calibration using capacitors of known capacitance. From the fit we obtain $T_0 = (4.946 \pm 0.001)$ μs, $d_0 = (1.332 \pm 0.001)$ mm, and $\beta = (0.035 \pm 0.001)$ μs mm. Since $\beta = \ln(3) R \epsilon_0 A$, we estimate the effective diameter of the probe tip to be roughly $D_{eff} = (4.8 \pm 0.1)$ mm. This is about a factor of 6 larger than the actual diameter of the probe tip, measured to be $D_{act} = (0.8 \pm 0.1)$ mm. In fact, this discrepancy is not surprising, because the precise geometry of the probe tip cannot be known *a priori* and, as a consequence, validity of the parallel-plate model does not hold (i.e., $D_{act} \neq D_{eff}$). The calibration involving a parallel-plate system is an interesting subject in its own right and enables critical assessments of a finite degree of parallelism manifested by a possible deviation from the expected power law.[7,13]

IV. TEMPERATURE DRIFTS

We have found a striking correlation between capacitance and temperature. The tip-sample capacitance at a fixed position, as measured by the period of the relaxation oscillator, is shown to be inversely proportional to the temperature of the op-amp, as measured by the resistance of a 10 kΩ thermistor. This behavior is clearly seen in Fig. 4. The dotted line corresponds to the resistance of a thermistor mounted inside the relaxation oscillator circuit box during a 12 day period. The actual relationship between the resistance of the thermistor and temperature is rather complicated.[14] But, to give a rough estimate, we have $\Delta T_C/\Delta R \sim 2\,^\circ$C/k$\Omega$ at room temperature ($\sim 20\,^\circ$C), translating into a $2\,^\circ$C change over the course of the 12 day period. This variation in temperature then corresponds to a $\Delta C = 0.3$ pF change in capacitance.

To suppress the temperature-driven fluctuations, it is possible to implement a temperature control system in which one side of the op-amp is in contact with a thermoelectric coupler (TEC), while the other side is in contact with a heat sink. A proportional-integral-derivative (PID) controller then actively stabilizes the system to a set temperature. Building a

This article is copyrighted as indicated in the article. Reuse of AAPT content is subject to the terms at: http://scitation.aip.org/termsconditions. Downloaded to IP: 66.194.72.20 On: Thu, 22 Jan 2015 23:42:23

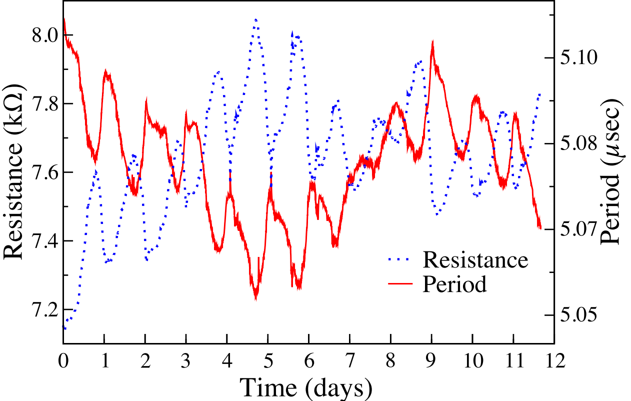

Fig. 4. Plot of thermistor resistance (i.e., temperature, dotted blue) and period (i.e., capacitance, solid red) data over the course of 12 days, displaying a strong correlation between them. As a result, a small drift of room temperature (approximately 2 °C change over the 12 day period) strongly affects the capacitance measurements. For temperature measurements, we have used a thermistor (TH10k, Thorlabs) whose resistance is inversely proportional to temperature (Ref. 11). Hence, the actual temperature and the capacitance are positively correlated.

PID controller circuit is relatively simple and provides great stability (∼10 mK).[15]

In the absence of a temperature-stabilizing mechanism, it becomes necessary to quantify the degree of correlation to account for any temperature-driven capacitance drift. Because a typical surface scan (in the non-contact mode) could take several hours, we focus on the capacitance-temperature fluctuation over a 15 h period (top of Fig. 5) and obtain the linear correlation coefficient (bottom of Fig. 5) using the definition[16] $r \equiv \sigma_{xy}/(\sigma_x \sigma_y)$, where $\sigma_{xy} = \sum(x_i - \bar{x})(y_i - \bar{y})/N$ is the covariance of x (period) and y (resistance), while $\sigma_x = \sqrt{\sum(x_i - \bar{x})^2}$ and $\sigma_y = \sqrt{\sum(y_i - \bar{y})^2}$ represent the standard deviations of x and y, respectively, with each sum running over N measurements. The obtained linear correlation coefficient is 0.99 with a best slope of 18.5kΩ/μs, or in terms of the actual unit of capacitance and temperature, 0.2pF/°C. This slope can then be directly used to correct any temperature-driven fluctuations. In our experiment, we have used a commercially available temperature controller system (TED 200C from Thorlabs), which provides excellent temperature stability of 2 mK. Based on this stability, the capacitance fluctuation due to temperature drifts is less than 2 fF (f=10^{-15}) and is ignored in the subsequent imaging results.

V. SCANNING RESULT I: NON-CONTACT MODE

Presented in Fig. 6 is the result of scanning over a sample of brass machined with the letters "S" and "U" (for Seattle University). The two letters are convex-shaped with a depth of 2 mm. For this particular scan, a paper clip is used as a probe tip and moves across the entire sample at a constant height in two dimensions (5 mm × 4 mm). Hence, the variation in capacitance is directly caused by the change in depth in the sample itself and represents a topographical map of the sample surface. Data are collected approximately every 100 μm for a total of 7200 points.

The main advantage of this method is that the tip and the sample never come in direct contact. Reliable scans are obtained as long as the tip-sample distance is kept

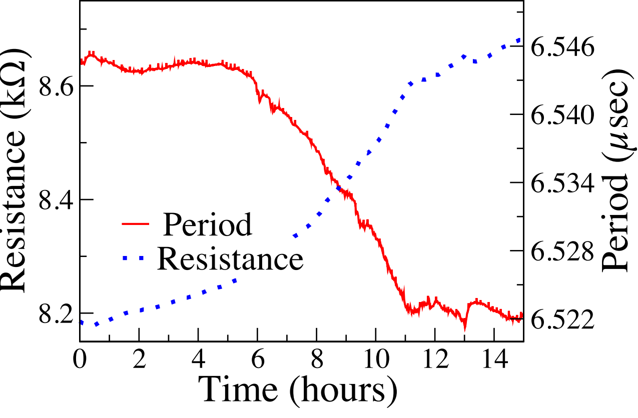

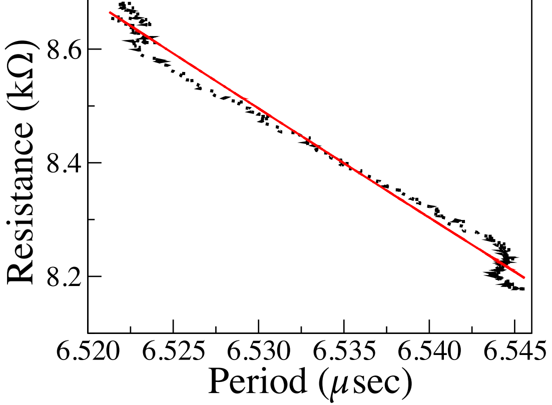

Fig. 5. A closer look at the temperature-capacitance correlation over a 15 h period. The top graph plots both resistance and period over time to show the inverse relationship between them, while the lower graph plots them against each other to extract the linear correlation coefficient, which is calculated to be $|r| = 0.99$ with a slope of (18.5 ±0.1) kΩ/μs. The variation in period during 15 h corresponds to an overall change in capacitance of 0.05 pF.

sufficiently small (<50 μm). Although the method is completely "touch-free" and thus non-destructive, several disadvantages also exist. First, as we have previously discussed, the effect of the temperature drift over time causes the capacitance to fluctuate. The capacitance fluctuation is quite inevitable in the non-contact method, and either active temperature stabilization or off-line treatment of data using

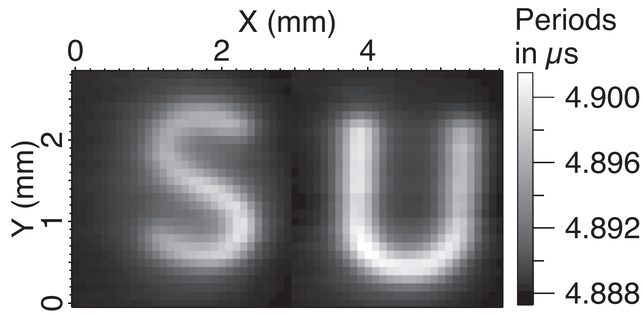

Fig. 6. Surface plot of a two-dimensional scan in constant-height mode. The probe tip is held at a fixed height and the stage containing the sample is moved in relation to it. Capacitance (period) measurements are conducted at regularly spaced intervals. The capacitance data directly correspond to height variations and subsequently produces a topographical map of the sample being scanned. The distance between pixels (i.e., lateral resolution) is 100 μm. A clear contrast of depth is obtained, with the letters "SU" distinctly resolved.

This article is copyrighted as indicated in the article. Reuse of AAPT content is subject to the terms at: http://scitation.aip.org/termsconditions. Downloaded to IP: 66.194.72.20 On: Thu, 22 Jan 2015 23:42:23

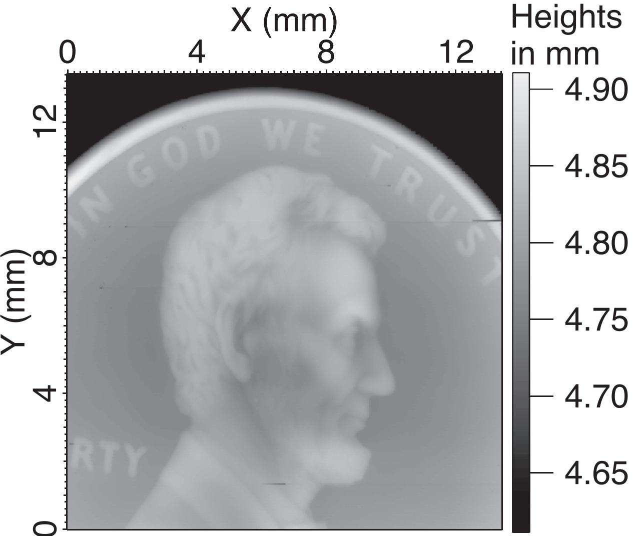

Fig. 7. Surface plot of a two-dimensional scan of a US penny in contact mode. At a given lateral position, the probe tip comes into physical contact with a point on the sample surface. The heights at which the capacitance (period) value rapidly falls are recorded and subsequently generate a topographical map of the sample. This method is somewhat slower, but yields much better resolution, because it is insensitive to externally driven fluctuations. The distance between each pixel is 45 μm for this run.

the linear correlation coefficient becomes necessary. Second, the system is extremely susceptible to acoustic disturbance. For example, the period measurement can be affected by something as minor as a person walking within a few feet of the experimental setup. It might be useful to place the setup inside an enclosure on a vibration-control table, but our scanning setup sat on an optical table without any enclosure. Finally, it is significantly less capable of scanning sharp cliffs or valleys in a sample, because the probe tip is not only interacting with the section of the sample immediately below it, but also with portions of the sample in the immediate vicinity of the relevant point. Depending on the topography of the sample, the surrounding (secondary) portion of the sample may be much closer to the tip than the relevant (primary) portion of the sample to be imaged, leading to an inflated period measurement.

VI. SCANNING RESULT II: CONTACT MODE

Results of the contact-mode method are shown in Figs. 7 and 8 as two-dimensional scans over the face of Abraham Lincoln on a US penny and the spaceship of a US-Florida quarter. This method actually brings the probe tip into direct contact with the sample. Our procedure is to (i) record the height at which a sharp fall in period measurements occurs; (ii) retract the tip a set distance away from the initial location, usually about 1 μm; and (iii) approach a new point to find the height at which the sharp fall occurs at that location. The procedure is repeated until a full, topological map of height variations is acquired over the entire surface of a sample.

The main advantage to this method is that it is significantly more precise and reliable than the non-contact method. While the non-contact method is extremely vulnerable to external noises, the contact method is almost impervious to them, making it drift-free. In this method, the *contrast* resolution and *lateral* resolution are limited by the resolution

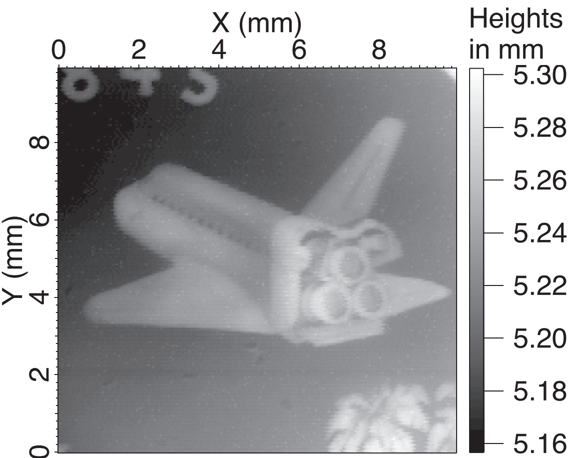

Fig. 8. Surface plot of a two-dimensional scan of a US quarter (Florida) in contact mode. The spaceship has been scanned with the same spatial resolution (45 μm) as in Fig. 7.

of the linear actuation (50 nm) and the size of the employed tip (2 μm), respectively. However, one major disadvantage is that, owing to the probe tip making repeated contacts with the sample surface, the end tip will blunt over time and, consequently, the lateral resolution degrades as the scanning progresses. Additionally, delicate portions of the sample could be damaged by the light, yet frequent, touch of the probe tip.

In principle, the capacitance measurement is not necessary to perform contact-mode microscopy. The only requirement is the capability to measure the contact transition when a sharp tip "touches" the surface of a sample. For this reason, a simple, battery-operated current-meter can be built to replace the present relaxation oscillator. There, the contrast resolution is still set by the minimum distance of the z-axis translation, and the lateral resolution is still limited by the size of the probe tip.

VII. CONCLUSION

We have reported results of scanning capacitance microscopy using a relaxation oscillator. Surface topography of both machined grooves and coins has been successfully obtained in the non-contact and contact modes with a spatial resolution of 100 μm and 45 μm, respectively. Our simple approach provides an excellent opportunity for students wishing to gain laboratory exposure to basic scanning probe imaging techniques at low cost (see Appendix A). To advance the present technique to the next level, the linear mechanical actuators can be replaced by a set of pico-meter piezoelectric translators (PZTs), and the tungsten probe tip can be attached with a template-assisted, electrochemically synthesized nanowire whose diameter is as small as 10 nm.[12] Despite some apparent challenges, such as manipulating an individual nanowire for attachment and maintaining a sharp-contact point, the ultra-small tip, aided by high-precision PZTs, is within experimental reach and could dramatically improve the presently achieved resolution by more than three orders of magnitude.

ACKNOWLEDGMENTS

This work was supported by the Clare Luce Boothe Research Program (M.P.), the M. J. Murdock Charitable

This article is copyrighted as indicated in the article. Reuse of AAPT content is subject to the terms at: http://scitation.aip.org/termsconditions. Downloaded to IP: 66.194.72.20 On: Thu, 22 Jan 2015 23:42:23

Trust, Pat and Mary Welch (S.T. and A.H.), and the Research at Undergraduate Institutions program through the National Science Foundation: PHY1307150 (W.J.K.). The authors also thank Charlie Rackson for careful proofreading of their manuscript.

APPENDIX A: COST AND TIME ESTIMATES FOR CONSTRUCTION OF THE SCM

The actual "probe" circuit costs less than \$20, since it is just a single operational amplifier (i.e., LM7171). The two most expensive components in our experiment are perhaps the three-axis XYZ stage and the servo controller driving the stage. Although our XYZ stage is constructed with three individual actuators (like two Z825 BV and Z812BV), it might be cheaper to buy an entire set together like MAX 343 and a motor driver BSC203 from Thorlabs, all of which cost about \$5000. Other essential components for construction of our experiment include a DAQ module equipped with timer/counter features (~\$1500) and an optical table (~\$500). A temperature controller might be useful, but it is not at all necessary for the contact mode operation. Even for the non-contact mode operation, an offline drift-correction could be applied after obtaining the temperature-capacitance correlation profile using a thermistor (Th10k, ~\$10). Assuming that a PC with MATLAB or other similar software is already available, the total cost of construction is less than \$8000. A three-axis stage with a controller is quite useful and could be employed in other experimental projects requiring precision positioning, which makes the purchase a wise investment. The present experiment could be completed over a two-month period during summer by one or two undergraduate students. The most time-consuming activity is writing MATLAB codes for stage positioning, without which the experiment could be finished within two weeks; essentially, once the oscillator is built and functioning as demonstrated in Fig. 1, that completes the construction of a SCM "sensor."

APPENDIX B: NOTES ON THE POWER-LAW FIT

From Eq. (4), the period equation of a parallel-plate capacitor can be fit to a functional form

$$T = T_0 + \frac{\beta}{d_r - d_0}, \tag{B1}$$

where $\beta \equiv 2\ln(3)R\epsilon_0 A$ and $T_0 \approx 2\ln(3)RC_{\text{para}}$. The power-law exponent γ is assumed to be unity for a parallel-plate system. Apart from β and T_0, there is an additional fit parameter d_0, representing the point of "hard contact." Notice that our linear actuator records only the relative distance d_r. That is, on the display panel of the actuator, the only information we get is how much distance the actuator will cover, not the actual gap separation between the tip and the sample surface. For this reason, d_0 plays a crucial role by converting the relative distance moved by the actuator to the absolute gap distance d from the definition implied in Eq. (B1): $d \equiv d_r - d_0$. Note that the asymptotic limit of "hard contact" occurs as the separation between the probe tip and the surface of a sample closes. In other words, the capacitance of the tip-sample surface rapidly increases in accordance with the $1/d$ power law. For systems obeying different power laws of capacitive interactions, refer to Ref. 17.

[a]Electronic mail: kimw@seattleu.edu

[1]J. R. Mately and J. Blanc, "Scanning capacitance microscopy," J. Appl. Phys. **57**, 1437–1444 (1985).

[2]C. C. Wiiliams, W. P. Hough, and S. A. Rishton, "Scanning capacitance microscopy on a 25 nm scale," Appl. Phys. Lett. **55**, 203–205 (1989).

[3]R. Stephenson, A. Verhulst, P. de Wolf, M. Caymax, and W. Vandervorst, "Contrast reversal in scanning capacitance microscopy imaging," Appl. Phys. Lett. **73**, 2597–2599 (1998).

[4]C. C. Wiiliams, J. Slinkman, W. P. Hough, and H. K. Wickramasinghe, "Lateral dopant profiling on a 100 nm scale by scanning capacitance microscopy," J. Vac. Sci. Technol. A **8**, 895–898 (1990).

[5]F. Giannazzo, F. Priolo, V. Raineri, and V. Privitera, "High-resolution scanning capacitance microscopy of silicon devices by surface beveling," Appl. Phys. Lett. **76**, 2565–2567 (2000).

[6]A. Hazeghi, J. A. Sulpizio, G. Diankov, D. Goldhaber-Gordon, and H. S. P. Wong, "An integrated capacitance bridge for high-resolution, wide temperature range quantum capacitance measurements," Rev. Sci. Instrum. **82**, 053904 (2011).

[7]A. Hankins, C. Rackson, and W. J. Kim, "Photon charge experiment," Am. J. Phys. **81**, 436–441 (2013).

[8]S. K. Lamoreaux, "Demonstration of the Casimir force in the 0.6 to 6 μm range," Phys. Rev. Lett. **78**, 5–8 (1997).

[9]A. R. Hambley, *Electronics*, 2nd ed. (Prentice Hall, Upper Saddle River, NJ, 2000), pp. 809–811.

[10]Y. Liu, S. Chen, M. Nakayama, and K. Watanabe, "Limitations of a relaxation oscillator in capacitance measurements," IEEE Trans. Instrum. Meas. **49**, 980–983 (2000).

[11]An analytical expression for the resistance-to-temperature conversion is available in the spec sheet available at <http://www.thorlabs.com>.

[12]W. J. Kim, S. Carr, and M. Wybourne, "Direct contact buckling of electrochemically grown gold nanowires," Appl. Phys. Lett. **87**, 173112 (2005).

[13]P. McDonnell, T. Graveson, C. Rackson, and W. J. Kim, "A detailed study of scaling behavior in electrochemical etching of tungsten wires," J. Phys. Chem. Solids **74**, 30–34 (2013).

[14]Thorlabs manual at <http://www.thorlabs.com>.

[15]K. G. Libbrecht and A. W. Libbrecht, "A versatile thermoelectric temperature controller with 10 mK reproducibility and 100 mK absolute accuracy," Rev. Sci. Instrum. **80**, 126107 (2009).

[16]J. R. Taylor, *Introduction to Error Analysis: The Study of Uncertainties in Physical Measurements*, 2nd ed. (University Science Books, Sausalito, CA, 1997), pp. 215–218.

[17]W. J. Kim and U. D. Schwarz, "Potential contributions of non contact atomic force microscopy for the future Casimir force measurements," J. Vac. Sci. Technol. B **28**, C4A1–C4A7 (2010).

This article is copyrighted as indicated in the article. Reuse of AAPT content is subject to the terms at: http://scitation.aip.org/termsconditions. Downloaded to IP: 66.194.72.20 On: Thu, 22 Jan 2015 23:42:23